J Comput Aided Mol Des (2011) 25:837–853
DOI 10.1007/s10822-011-9467-4

Conformational analysis of the $MBP_{83–99}$ (Phe^{91}) and $MBP_{83–99}$ (Tyr^{91}) peptide analogues and study of their interactions with the HLA-DR2 and human TCR receptors by using Molecular Dynamics

C. Potamitis · M.-T. Matsoukas · T. Tselios · T. Mavromoustakos · S. Golič Grdadolnik

Received: 10 September 2010 / Accepted: 17 August 2011 / Published online: 6 September 2011

Abstract The two new synthetic analogues of the $MBP_{83–99}$ epitope substituted at Lys^{91} (primary TCR contact) with Phe [$MBP_{83–99}$ (Phe^{91})] or Tyr [$MBP_{83–99}$ (Tyr^{91})], have been structurally elucidated using 1D and 2D high resolution NMR studies. The conformational analysis of the two altered peptide ligands (APLs) has been performed and showed that they adopt a linear and extended conformation which is in agreement with the structural requirements of the peptides that interact with the HLA-DR2 and TCR receptors. In addition, Molecular Dynamics (MD) simulations of the two analogues in complex with HLA-DR2 (DRA, DRB1*1501) and TCR were performed. Similarities and differences of the binding motif of the two analogues were observed which provide a possible explanation of their biological activity. Their differences in the binding mode in comparison with the $MBP_{83–99}$ epitope may also explain their antagonistic versus agonistic activity. The obtained results clearly indicate that substitutions in crucial amino acids (TCR contacts) in combination with the specific conformational characteristics of the $MBP_{83–99}$ immunodominant epitope lead to an alteration of their biological activity. These results make the rational drug design intriguing since the biological activity is very sensitive to the substitution and conformation of the mutated MBP epitopes.

Keywords Molecular Dynamics (MD) · Myelin basic protein (MBP) · Conformational analysis · Binding motif · NMR · Multiple sclerosis (MS)

Electronic supplementary material The online version of this article (doi:10.1007/s10822-011-9467-4) contains supplementary material, which is available to authorized users.

C. Potamitis · T. Mavromoustakos
National Hellenic Research Foundation, Institute of Organic and Pharmaceutical Chemistry, Vas. Constantinou 48, 11635 Athens, Greece

C. Potamitis · T. Mavromoustakos (✉)
Chemistry Department, University of Athens, Panepistimiopolis, Zographou, 15784 Athens, Greece
e-mail: tmavrom@chem.uoa.gr

M.-T. Matsoukas · T. Tselios (✉)
Department of Chemistry, University of Patras, Patras 26500, Greece
e-mail: ttselios@upatras.gr

S. Golič Grdadolnik
Laboratory of Biomolecular Structure, National Institute of Chemistry, Hajdrihova 19, 1001 Ljubljana, Slovenia

S. Golič Grdadolnik (✉)
EN-FIST Centre of Excellence, Dunajska 156, 1000 Ljubljana, Slovenia
e-mail: simona.grdadolnik@ki.si

Introduction

Multiple sclerosis (MS) is an inflammatory disease, characterized by the demyelination of the white matter of the central nervous system (CNS). It is caused by aberrant responses of autoreactive T-cells that escape negative selection [1, 2]. T-cell receptors (TCRs) recognize self-peptide fragments bound to major histocompatibility complex II (MHC II) molecules (in human referred to as HLA, Human Leukocyte Antigens). This recognition results in T-cell activation and proliferation and the triggering of an autoimmune response [3, 4]. It is well known that MBP epitopes induce in mice experimental autoimmune encephalomyelitis (EAE), the best studied animal model of MS [7, 8, 10, 11, 12].

Reported work has demonstrated that the HLA-DR2 (DRA, DRB1*1501) haplotype is present at an increased

frequency in northern European caucasoid patients with MS [5, 6]. Although the antigenic components of myelin in MS have not been identified with certainty, myelin basic protein (MBP) is believed to be the main candidate autoantigen, and more specifically $MBP_{83–99}$ shows the strongest binding with HLA-DR2 compared to other MBP epitopes. $MBP_{83–99}$ interacts with HLA-DR2 through hydrophobic interactions with amino acids Val^{87} and Phe^{90}, while the amino acids that interact with TCR are His^{88}, Phe^{89} and Lys^{91} [7–9].

In a previous study, the solution structural motif of $MBP_{83–99}$ has been performed using 2D ^{1}H-NMR spectroscopy in dimethyl sulfoxide (DMSO). A rather extended conformation, along with the formation of a well defined α-helix spanning residues Val^{87}-Phe^{90} is proposed, as no long-range correlations were observed. Moreover, the residues of $MBP_{87–99}$ peptide analogues which are important for T-cell receptor recognition are found to be solvent exposed [13].

Two phase II clinical trials using an altered peptide ligand (APL) derived from the $MBP_{83–99}$ have been reported [14, 15]. Their biological data urged for the synthesis of more novel analogues with a better biological profile. Two analogues have been designed and synthesized in which the Lys^{91} is substituted with Phe or Tyr. This amino acid has been chosen for mutation because it plays a crucial role in the recognition of the epitope by TCR (Fig. 1).

Fig. 1 Structures of the wild type $MBP_{83–96}$ (the numbering is in accordance with the human MBP [35]) and the two new synthetic analogues of the $MBP_{83–99}$ epitope substituted at Lys^{91} amino acid with Phe ($MBP_{83–99}$ (Phe^{91})) or Tyr ($MBP_{83–99}$ (Tyr^{91}))

The obtained biological results of mutated $MBP_{83–99}$ analogues with crucial T-cell receptor (TCR) substitution at position 91 (Lys) were promising. The $MBP_{83–99}$ (Phe^{91}) and $MBP_{83–99}$ (Tyr^{91}) analogues were evaluated in SJL/J mice emulsified in complete Freund's adjuvant (CFA) [16]. Immunized mice with $MBP_{83–99}$ (Phe^{91}) analogue generated moderate levels of IFN-γ, while with $MBP_{83–99}$ (Tyr^{91}) were negative. However, the linear peptides resulted in non-cross reactivity by T-cells against native $MBP_{83–99}$ epitope [16]. Furthermore, the linear $MBP_{83–99}$ (Phe^{91}) and $MBP_{83–99}$ (Tyr^{91}) peptide analogues conjugated to reduced mannan were immunized in SJL/J mice [17]. It was found that these peptides-mannan conjugations induce T cell responses with the induction of high level of IL-4 while only the $MBP_{83–99}$ (Phe^{91}) peptide generated IFN-γ secreting T cells. Moreover, high antibody levels were induced by $MBP_{83–99}$ (Tyr^{91}) and low by $MBP_{83–99}$ (Phe^{91}) peptides [17]. A very significant observation is that these peptides did not cross-react with native MBP protein at 1/200 and 1/1,600 sera dilution [17]. The $MBP_{83–99}$ (Tyr^{91}) peptide on reduced mannan gave the best cytokine and antibody profile and constitutes a promising candidate peptide for the immunotherapy of Multiple Sclerosis (MS) [17, 18].

The differential and promising biological properties shown by the two peptidic analogues triggered our research interest to study their conformational and binding properties to HLA-DR2. Such studies reveal not only the crucial interactions between the epitope and the receptor, but also aid in the designing novel analogues with better biological profile.

Our laboratory has been engaged for the last decade in the use of the powerful NMR spectroscopy that is well known to be a capable technique to study the putative bioactive conformers of biologically important molecules and specifically MBP epitopes. NMR spectroscopy is coupled with MD simulations to study the binding motif of the altered peptide epitopes of $MBP_{83–99}$ with HLA-DR2 [19–31].

Results and discussion

Structure identification and conformational analysis

The chemical shifts of the protons and carbon-13 of the two peptides $MBP_{83–99}$ (Phe^{91}) and $MBP_{83–99}$ (Tyr^{91}) were achieved with the aid of the combined use of ^{1}H-NMR, 2D-TOCSY, 2D-NOESY and 2D-HSQC spectra in DMSO-d_6 solvent, as it provides an amphiphilic environment, mimicking the physiological conditions at the receptor binding site [32] (Supporting information, Tables S1 and S2, Figures SF1–SF12).

The proton–proton NOE connectivities were identified from 2D NOESY spectra acquired using Varian 800 MHz at 25 °C and mixing time of 75 ms (Tables 1, 2). Along the entire backbone of the two peptides strong sequential NOE connectivities $d_{\alpha N(i,i+1)}$ are observed. These are indicating a predominant population of extended backbone conformation in DMSO-d_6 solvent. In contrast to wild type $MBP_{83–99}$, no secondary structure elements or backbone local folded structures can be identified in DMSO-d_6 solvent as the indicative medium or long range contacts of the two peptides are absent.

The difference in the chemical shifts between Cβ-Cγ of the three Pro was found to be 4.4–4.5 ppm, showing preferred *trans* conformation for Asn^{84}–Pro^{85}, Thr^{95}–Pro^{96} and Thr^{98}–Pro^{99} bonds [33].

Comparative solution NMR studies

Recently the crystallographic structure (PDB code: 1YMM) of the trimolecular complex between the $MBP_{83–96}$, HLA-DR2 (DRA, DRB1*1501) and a human TCR isolated from a patient with relapsing-remitting MS was reported [34]. In this complex, the $MBP_{83–96}$ peptide adopted an extended conformation with His^{88}, Phe^{89} and Lys^{91} residues to constitute the major TCR contact residues for human MBP-specific T-cell clones which are solvent exposed and accessible for recognition by TCR [34].

Table 1 NOE intensities for peptide $MBP_{83–99}$ (Phe^{91}) in DMSO-d_6 solution

	Glu 83	Asn 84	Pro 85	Val 86	Val 87	His 88	Phe 89	Phe 90	Phe 91	Asn 92	Ile 93	Val 94	Thr 95	Pro 96	Arg 97	Thr 98	Pro 99
$d_{NN(i,i+1)}$																	
$d_{\alpha N(i,i+1)}$																	
$d_{\beta N(i,i+1)}$																	
$d_{\gamma N(i,i+1)}$																	
$d_{\alpha\delta(i,i+1)}$																	
$d_{\gamma\delta(i,i+1)}$																	

Strong (< 2.5 Å)
Medium (2.5–3.7 Å)
Weak (3.7–5.0 Å)

Table 2 NOE intensities for peptide $MBP_{83–99}$ (Tyr^{91}) in DMSO-d_6

	Glu 83	Asn 84	Pro 85	Val 86	Val 87	His 88	Phe 89	Phe 90	Tyr 91	Asn 92	Ile 93	Val 94	Thr 95	Pro 96	Arg 97	Thr 98	Pro 99
$d_{NN(i,i+1)}$																	
$d_{\alpha N(i,i+1)}$																	
$d_{\beta N(i,i+1)}$																	
$d_{\beta N(i,i+2)}$																	
$d_{\gamma N(i,i+1)}$																	
$d_{\alpha\delta(i,i+1)}$																	
$d_{\gamma\delta(i,i+1)}$																	
$d_{\alpha\gamma(i,i+1)}$																	
$d_{\beta\delta(i,i+1)}$																	
$d_{\gamma\delta(i,i+1)}$																	
$d_{R\beta(i,i+1)}$																	
$d_{R\beta(i,i+2)}$																	
$d_{\gamma R(i,i+2)}$																	

Strong (< 2.5 Å)
Medium (2.5–3.7 Å)
Weak (3.7–5.0 Å)

Spyranti et al. published data using high resolution NMR spectroscopy in DMSO-d_6 solution for $MBP_{83–99}$ peptide and observed some local bending in the His^{88}–Phe^{90}, Asn^{92}–Thr^{95} and α-helix spanning residues Val^{87}–Phe^{90} [13]. Fares et al. published results for the MBP_{81-98}, showing that this epitope forms a stable, amphipathic, alpha helix under organic and membrane-mimetic conditions, but has only a partially helical conformation in aqueous solution [35]. Results obtained by Spyranti et al. [13] resembled more to ours. This is expected, since Spyranti et al. used DMSO-d_6 solvent like ours, while Fares et al. used either aqueous solution or mixture of TFE and water or dispersion of 100 mM dodecylphosphocholine.

Insofar, in all our NMR studies performed in DMSO-d_6 solution linear APLs for the epitopes $MBP_{83–99}$ and $MBP_{87–99}$ showed predominant extended conformations [22, 23, 26].

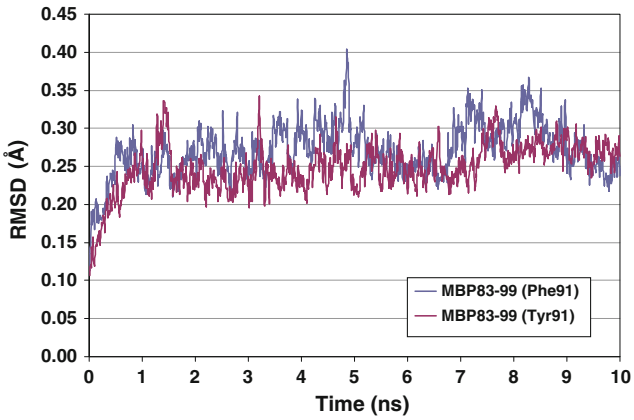

Fig. 2 Fluctuation of the RMSD values of the peptides $MBP_{83–99}$ (Phe^{91}) and $MBP_{83–99}$ (Tyr^{91}) versus the simulation time of Molecular Dynamics

Molecular Dynamics results of the two peptides on the trimolecular complex of $MBP_{83–96}$, HLA-DR2 (DRA, DRB1*1501) and a human TCR

2D NOESY experiments revealed no long range NOEs for the two peptides under study, implying an extended conformation in DMSO-d_6 solution. Thus, the extended crystal structure of $MBP_{83–96}$ was modified to the altered peptides of $MBP_{83–99}$ and minimized. These structures were in accordance to the observation of strong sequential $d_{\alpha N(i,i+1)}$ NOE connectivities and the absence of long range NOEs. The two peptides under study were then docked in the pocket of the native peptide $MBP_{83–96}$.

The best docking poses for each peptide were subjected to Molecular Dynamics. RMSD values derived by comparison of the corresponding heavy atoms of the two peptides versus simulation time indicate that after 1 ns both of them have reached to a plateau (Fig. 2). The fluctuation of the RMSD values for both peptides is around 0.15 Å.

A total of 1,000 conformers from the trajectory file were divided into 5 families according to their RMSD values based on heavy atoms. The trimolecular complexes for the lowest energy conformer from each cluster were subjected to Truncated Newton Conjugate Gradient (TNCG) minimization. The hydrogen bonds, hydrophobic and electrostatic interactions from the 5 conformers in the trimolecular complex are shown in Tables 3 and 4.

Table 3 Hydrogen bonds, hydrophobic and electrostatic interactions between the five conformers of $MBP_{83-99}(Phe^{91})$ and the proteins HLA-DR2 and TCR of the trimolecular complex

Residues		Interactions														
$MBP_{83–99}$ (Phe^{91})	Receptor	Hydrogen bonds					Hydrophobic					Electrostatic				
		Conformers					Conformers					Conformers				
		1	2	3	4	5	1	2	3	4	5	1	2	3	4	5
Glu 83	HLA-DR2α Phe51	✔	✘	✘	✘	✘	✘	✘	✘	✘	✘	✘	✘	✘	✘	✘
Glu 83	TCR-Vα Lys99	✘	✔	✔	✔	✔	✘	✘	✘	✘	✘	✘	✔	✔	✔	✔
Glu 83	TCR-Vα Thr97	✘	✘	✔	✘	✔	✘	✘	✘	✘	✘	✘	✘	✘	✘	✘
Glu 83	TCR-Vβ Glu59	✘	✔	✔	✘	✘	✘	✘	✘	✘	✘	✘	✘	✘	✘	✘
Glu 83	TCR-Vβ Gln60	✘	✘	✘	✘	✔	✘	✘	✘	✘	✘	✘	✘	✘	✘	✘
Asn 84	TCR-Vα Lys99	✔	✘	✘	✘	✘	✘	✘	✘	✘	✘	✘	✘	✘	✘	✘
Asn 84	TCR-Vα Ala52	✘	✘	✔	✘	✘	✘	✘	✘	✘	✘	✘	✘	✘	✘	✘
Asn 84	TCR-Vβ Tyr58	✔	✘	✘	✘	✘	✘	✘	✘	✘	✘	✘	✘	✘	✘	✘
Asn 84	TCR-Vβ Glu59	✔	✘	✘	✘	✘	✘	✘	✘	✘	✘	✘	✘	✘	✘	✘
Asn 84	HLA-DR2α Phe51	✘	✘	✘	✘	✔	✘	✘	✘	✘	✘	✘	✘	✘	✘	✘
Pro 85	HLA-DR2α Ser53	✔	✔	✔	✔	✔	✘	✘	✘	✘	✘	✘	✘	✘	✘	✘
Pro 85	HLA-DR2α Phe51	✘	✘	✘	✘	✘	✔	✘	✘	✘	✘	✘	✘	✘	✘	✘
Pro 85	HLA-DR2α Ala52	✘	✘	✘	✘	✘	✔	✘	✘	✔	✘	✘	✘	✘	✘	✘
Pro 85	HLA-DR2β Val85	✘	✘	✘	✘	✘	✔	✘	✘	✔	✘	✘	✘	✘	✘	✘
Pro 85	TCR-Vα Thr97	✘	✘	✘	✘	✘	✔	✘	✘	✘	✘	✘	✘	✘	✘	✘
Val 86	TCR-Vα Gly96	✔	✔	✔	✔	✔	✘	✘	✘	✘	✘	✘	✘	✘	✘	✘
Val 86	TCR-Vα Thr97	✘	✘	✘	✘	✘	✔	✔	✔	✔	✔	✘	✘	✘	✘	✘
Val 86	TCR-Vα Tyr98	✘	✘	✘	✘	✘	✔	✔	✔	✔	✔	✘	✘	✘	✘	✘
Val 86	TCR-Vβ Tyr58	✘	✘	✘	✘	✘	✘	✔	✘	✔	✔	✘	✘	✘	✘	✘
Val 86	HLA-DR2β His81	✘	✔	✘	✘	✘	✘	✘	✘	✘	✘	✘	✘	✘	✘	✘
Val 87	HLA-DR2β Val85	✘	✘	✘	✘	✘	✔	✔	✔	✔	✔	✘	✘	✘	✘	✘
Val 87	HLA-DR2β Val86	✘	✘	✘	✘	✘	✘	✔	✘	✘	✘	✘	✘	✘	✘	✘
Val 87	HLA-DR2α Phe32	✘	✘	✘	✘	✘	✔	✔	✔	✔	✔	✘	✘	✘	✘	✘
Val 87	HLA-DR2α Trp43	✘	✘	✘	✘	✘	✔	✔	✔	✔	✘	✘	✘	✘	✘	✘
Val 87	HLA-DR2α Phe54	✘	✘	✘	✘	✘	✔	✔	✔	✘	✔	✘	✘	✘	✘	✘
Val 87	HLA-DR2α Phe24	✘	✘	✘	✘	✘	✘	✔	✔	✔	✔	✘	✘	✘	✘	✘
Val 87	HLA-DR2α Ser53	✘	✔	✔	✔	✔	✘	✘	✘	✘	✘	✘	✘	✘	✘	✘
Val 87	TCR-Vα Tyr98	✘	✘	✘	✔	✔	✘	✘	✘	✘	✘	✘	✘	✘	✘	✘
His 88	HLA-DR2β Asn82	✔	✔	✔	✔	✔	✘	✘	✘	✘	✘	✘	✘	✘	✘	✘
His 88	HLA-DR2β His81	✘	✘	✘	✘	✘	✘	✘	✘	✘	✘	✘	✘	✔	✔	✔
His 88	TCR-Vβ Asn30	✘	✔	✘	✘	✘	✘	✘	✘	✘	✘	✘	✘	✘	✘	✘
His 88	TCR-Vβ Asn104	✘	✘	✘	✘	✘	✘	✘	✘	✘	✘	✘	✘	✔	✘	✘
His 88	TCR-Vβ Ala103	✘	✘	✘	✘	✘	✘	✘	✘	✘	✘	✘	✘	✘	✔	✔
Phe 89	TCR-Vβ Ala103	✔	✔	✔	✔	✔	✘	✘	✘	✘	✘	✘	✘	✘	✘	✔
Phe 89	TCR-Vβ Thr31	✘	✘	✘	✘	✘	✔	✔	✔	✔	✔	✘	✘	✘	✘	✘
Phe 89	HLA-DR2α Phe54	✘	✘	✘	✘	✘	✔	✔	✔	✔	✘	✘	✘	✘	✘	✘
Phe 89	HLA-DR2α Ala59	✘	✘	✘	✘	✘	✔	✔	✘	✘	✘	✘	✘	✘	✘	✘
Phe 90	HLA-DR2α Gln9	✔	✘	✔	✔	✔	✘	✘	✘	✘	✘	✘	✘	✘	✘	✘
Phe 90	HLA-DR2α Asn62	✔	✔	✘	✔	✔	✘	✘	✘	✘	✘	✘	✘	✘	✘	✘
Phe 90	HLA-DR2β Ile67	✘	✘	✘	✘	✘	✔	✘	✘	✘	✘	✘	✘	✘	✘	✘
Phe 90	HLA-DR2β Tyr 78	✘	✘	✘	✘	✘	✘	✘	✔	✘	✘	✘	✘	✘	✘	✘
Phe 90	HLA-DR2β Ala71	✘	✘	✘	✘	✘	✔	✔	✔	✔	✔	✘	✘	✘	✘	✘
Phe 90	HLA-DR2β Phe26	✘	✘	✘	✘	✘	✘	✔	✔	✔	✔	✘	✘	✘	✘	✘
Phe 90	HLA-DR2β Ala74	✘	✘	✘	✘	✘	✘	✔	✔	✘	✘	✘	✘	✘	✘	✘

Table 3 continued

Residues		Interactions														
MBP_{83-99} (Phe^{91})	Receptor	Hydrogen bonds					Hydrophobic					Electrostatic				
		Conformers					Conformers					Conformers				
		1	2	3	4	5	1	2	3	4	5	1	2	3	4	5
Phe 91	HLA-DR2β Gln70	✔	✘	✔	✔	✔	✘	✘	✘	✘	✘	✘	✘	✘	✘	✘
Phe 91	TCR-Vβ Thr100	✘	✘	✘	✘	✘	✔	✘	✔	✔	✔	✘	✘	✘	✘	✘
Asn 92	HLA-DR2α Asp66	✔	✘	✔	✔	✔	✘	✘	✘	✘	✘	✘	✘	✘	✘	✘
Asn 92	TCR-Vβ Thr100	✔	✘	✘	✘	✘	✘	✘	✘	✘	✘	✘	✘	✘	✘	✘
Asn 92	HLA-DR2β Trp61	✘	✔	✔	✔	✘	✘	✘	✘	✘	✘	✘	✘	✘	✘	✘
Asn 92	HLA-DR2β Tyr30	✘	✘	✘	✔	✘	✘	✘	✘	✘	✘	✘	✘	✘	✘	✘
Ile 93	HLA-DR2β Tyr60	✔	✔	✔	✘	✔	✘	✘	✘	✘	✘	✘	✘	✘	✘	✘
Ile 93	HLA-DR2β Ile67	✘	✘	✘	✘	✘	✔	✔	✔	✔	✔	✘	✘	✘	✘	✘
Ile 93	HLA-DR2β Trp61	✘	✘	✘	✘	✔	✘	✘	✘	✘	✘	✘	✘	✘	✘	✘
Val 94	HLA-DR2β Tyr60	✔	✔	✔	✔	✔	✘	✘	✘	✘	✘	✘	✘	✘	✘	✘
Val 94	HLA-DR2α Val65	✘	✘	✘	✘	✘	✔	✔	✔	✔	✔	✘	✘	✘	✘	✘
Val 94	HLA-DR2α Ala68	✘	✘	✘	✘	✘	✔	✔	✔	✔	✔	✘	✘	✘	✘	✘
Val 94	HLA-DR2α Ile72	✘	✘	✘	✘	✘	✔	✘	✔	✘	✘	✘	✘	✘	✘	✘
Thr 95	HLA-DR2α Asn69	✔	✔	✔	✔	✘	✘	✘	✘	✘	✘	✘	✘	✘	✘	✘
Thr 95	HLA-DR2α Arg76	✔	✘	✘	✘	✘	✘	✘	✘	✘	✘	✘	✘	✘	✘	✘
Thr 95	HLA-DR2β Asp57	✔	✔	✔	✔	✔	✘	✘	✘	✘	✘	✘	✘	✘	✘	✘
Thr 95	HLA-DR2α Ile72	✘	✘	✘	✘	✘	✔	✔	✔	✔	✔	✘	✘	✘	✘	✘
Thr 95	HLA-DR2α Met73	✘	✘	✘	✘	✘	✔	✔	✔	✔	✔	✘	✘	✘	✘	✘
Thr 95	HLA-DR2β Trp61	✘	✘	✘	✘	✘	✔	✔	✔	✔	✔	✘	✘	✘	✘	✘
Thr 95	HLA-DR2β Tyr60	✘	✘	✘	✘	✘	✘	✘	✘	✔	✔	✘	✘	✘	✘	✘
Pro 96	HLA-DR2α Arg76	✔	✔	✘	✔	✘	✘	✘	✘	✘	✘	✘	✘	✘	✘	✘
Pro 96	HLA-DR2β Tyr60	✘	✘	✘	✘	✘	✔	✔	✔	✔	✔	✘	✘	✘	✘	✘
Arg 97	HLA-DR2α Ile72	✘	✘	✘	✘	✘	✔	✘	✘	✘	✘	✘	✘	✘	✘	✘
Thr 98	HLA-DR2α Ile72	✘	✘	✘	✘	✘	✔	✔	✘	✘	✘	✘	✘	✘	✘	✘
Thr 98	HLA-DR2α Lys75	✘	✔	✘	✘	✘	✘	✘	✘	✘	✘	✘	✘	✘	✘	✘
Thr 98	HLA-DR2α Arg76	✘	✘	✔	✘	✔	✘	✘	✘	✘	✘	✘	✘	✘	✘	✘
Pro 99	HLA-DR2α Lys75	✘	✘	✘	✘	✘	✘	✘	✘	✔	✘	✘	✔	✔	✘	✘
Pro 99	HLA-DR2α Ile72	✘	✘	✘	✘	✘	✘	✘	✘	✔	✘	✘	✘	✘	✘	✘

The two chains of HLA-DR2 are denoted with α and β, and of TCR with Vα and Vβ

MD results for the peptide MBP_{83-99} (Phe^{91})

Figure 3 shows the hydrogen bond donors (green) and acceptors (red), the hydrophobic interactions (yellow) and electrostatic interactions (red: negative charged groups, blue: positive charged groups) of the most energetically favored conformer, 3 of MBP_{83-99} (Phe^{91}) during its binding with amino acids of the receptors HLA-DR2 and TCR as they are revealed from the application of MD.

More specifically, the amino acids Val^{87} and Phe^{90} of MBP_{83-99} (Phe^{91}) which are required for the binding of MBP_{83-99} to HLA-DR2, form hydrogen bonds with Ser^{53} and Gln^{9} of HLA-DR2α correspondingly. Furthermore, Phe^{90} forms hydrogen bonding with Asn^{62} of HLA-DR2α, not present in the conformer 3 (Tables 3 and 5) but its occurrence through the MD simulations is 81% (Table 6). In addition, Val^{87} develops hydrophobic interactions with amino acids Phe^{24}, Phe^{32}, Trp^{43} and Phe^{54} of HLA-DR2α and Val^{85} of HLA-DR2β, while Phe^{90} with amino acids Phe^{26}, Ala^{71}, Ala^{74} and Tyr^{78} of HLA-DR2β.

The interactions that are appearing during the recognition of MBP_{83-99} (Phe^{91}) with TCR are: (1) hydrogen bonds between Phe^{89} of the peptide MBP_{83-99} (Phe^{91}) and Ala^{103} of TCR-Vβ and between Val^{86} and Gly^{96} of the TCR-Vα, (2) hydrophobic interactions between Val^{86} of the peptide MBP_{83-99} (Phe^{91}) and Thr^{97} and Tyr^{98} of the TCR-Vα and between Phe^{89} and Thr^{31} TCR-Vβ. Interestingly, the mutated amino acid Phe^{91} forms hydrophobic interactions with Thr^{100} of TCR-Vβ and hydrogen bonding

Table 4 Hydrogen bonds, hydrophobic and electrostatic interactions between the five conformers of $MBP_{83–99}$ (Tyr^{91}) and the proteins HLA-DR2 and TCR of the trimolecular complex

Residues		Interactions														
$MBP_{83–99}$ (Tyr^{91})	Receptor	Hydrogen bonds					Hydrophobic					Electrostatic				
		Conformers					Conformers					Conformers				
		1	2	3	4	5	1	2	3	4	5	1	2	3	4	5
Glu 83	TCR-Vα Lys99	✘	✘	✘	✘	✔	✘	✘	✘	✘	✘	✔	✔	✘	✘	✘
Glu 83	TCR-Vα Thr97	✔	✘	✘	✘	✘	✘	✘	✘	✘	✘	✘	✘	✘	✘	✘
Glu 83	TCR-Vβ Glu59	✘	✔	✘	✔	✘	✘	✘	✘	✘	✘	✘	✘	✘	✘	✘
Glu 83	TCR-Vβ Gln60	✘	✔	✘	✘	✘	✘	✘	✘	✘	✘	✘	✘	✘	✘	✘
Glu 83	TCR-Vβ Tyr58	✔	✘	✔	✔	✔	✘	✘	✘	✘	✘	✘	✘	✘	✘	✘
Glu 83	TCR-Vβ Gly61	✘	✘	✔	✔	✘	✘	✘	✘	✘	✘	✘	✘	✘	✘	✘
Asn 84	TCR-Vβ Tyr58	✘	✔	✔	✔	✘	✘	✘	✘	✘	✘	✘	✘	✘	✘	✘
Asn 84	TCR-Vβ Glu59	✘	✔	✔	✘	✘	✘	✘	✘	✘	✘	✘	✘	✘	✘	✘
Asn 84	TCR-Vβ Phe51	✘	✘	✘	✔	✘	✘	✘	✘	✘	✘	✘	✘	✘	✘	✘
Asn 84	TCR-Vβ Thr97	✘	✘	✘	✔	✘	✘	✘	✘	✘	✘	✘	✘	✘	✘	✘
Asn 84	HLA-DR2α Ser53	✔	✘	✘	✘	✔	✘	✘	✘	✘	✘	✘	✘	✘	✘	✘
Asn 84	HLA-DR2α Arg50	✔	✘	✘	✘	✘	✘	✘	✘	✘	✘	✘	✘	✘	✘	✘
Pro 85	HLA-DR2α Ser53	✔	✔	✔	✔	✔	✘	✘	✘	✘	✘	✘	✘	✘	✘	✘
Pro 85	HLA-DR2β Val85	✘	✘	✘	✘	✘	✘	✘	✔	✘	✘	✘	✘	✘	✘	✘
Pro 85	TCR-Vα Thr97	✘	✘	✘	✘	✘	✘	✘	✔	✘	✘	✘	✘	✘	✘	✘
Val 86	TCR-Vα Gly96	✔	✔	✔	✔	✔	✘	✘	✘	✘	✘	✘	✘	✘	✘	✘
Val 86	TCR-Vα Thr97	✘	✘	✘	✘	✘	✔	✔	✔	✔	✔	✘	✘	✘	✘	✘
Val 86	TCR-Vα Tyr98	✘	✘	✘	✘	✘	✔	✔	✔	✔	✔	✘	✘	✘	✘	✘
Val 86	TCR-Vβ Tyr58	✘	✘	✘	✘	✘	✘	✘	✔	✘	✘	✘	✘	✘	✘	✘
Val 87	HLA-DR2β Val85	✘	✘	✘	✘	✘	✔	✔	✔	✔	✔	✘	✘	✘	✘	✘
Val 87	HLA-DR2β Val86	✘	✘	✘	✘	✘	✘	✔	✘	✔	✔	✘	✘	✘	✘	✘
Val 87	HLA-DR2α Trp43	✘	✘	✘	✘	✘	✔	✔	✘	✔	✘	✘	✘	✘	✘	✘
Val 87	HLA-DR2α Phe54	✘	✘	✘	✘	✘	✔	✔	✔	✔	✔	✘	✘	✘	✘	✘
Val 87	HLA-DR2α Phe24	✘	✘	✘	✘	✘	✘	✔	✔	✔	✔	✘	✘	✘	✘	✘
Val 87	HLA-DR2α Ser53	✔	✔	✔	✔	✔	✘	✘	✘	✘	✘	✘	✘	✘	✘	✘
Val 87	HLA-DR2α Ala52	✘	✘	✘	✘	✘	✔	✘	✔	✘	✔	✘	✘	✘	✘	✘
Val 87	HLA-DR2α Glu55	✘	✔	✔	✔	✔	✘	✘	✘	✘	✘	✘	✘	✘	✘	✘
His 88	HLA-DR2β Asn82	✔	✔	✔	✔	✔	✘	✘	✘	✘	✘	✘	✘	✘	✘	✘
His 88	HLA-DR2β His81	✘	✘	✘	✘	✘	✘	✘	✘	✘	✘	✔	✘	✘	✘	✘
His 88	TCR-Vα Asp92	✔	✘	✘	✘	✘	✘	✘	✘	✘	✘	✔	✘	✘	✘	✘
His 88	TCR-Vβ Ala103	✘	✘	✘	✘	✘	✔	✔	✘	✘	✘	✘	✘	✘	✘	✔
Phe 89	TCR-Vβ Ala103	✔	✔	✔	✔	✔	✔	✔	✘	✘	✘	✘	✘	✘	✘	✔
Phe 89	TCR-Vβ Thr31	✘	✘	✘	✘	✘	✘	✔	✔	✘	✔	✘	✘	✘	✘	✘
Phe 89	HLA-DR2α Ala59	✘	✘	✘	✘	✘	✔	✔	✘	✔	✔	✘	✘	✘	✘	✘
Phe 90	HLA-DR2α Gln9	✔	✘	✔	✔	✔	✘	✘	✘	✘	✘	✘	✘	✘	✘	✘
Phe 90	HLA-DR2α Asn62	✔	✔	✘	✘	✘	✘	✘	✘	✘	✘	✘	✘	✘	✘	✘
Phe 90	HLA-DR2β Tyr 78	✘	✘	✘	✘	✘	✔	✘	✔	✘	✘	✘	✘	✘	✘	✘
Phe 90	HLA-DR2β Ala71	✘	✘	✘	✘	✘	✔	✔	✔	✔	✔	✘	✘	✘	✘	✘
Phe 90	HLA-DR2β Phe26	✘	✘	✘	✘	✘	✔	✔	✔	✔	✔	✘	✘	✘	✘	✘
Phe 90	HLA-DR2β Ala74	✘	✘	✘	✘	✘	✔	✔	✔	✔	✔	✘	✘	✘	✘	✘
Phe 90	TCR-Vβ Ala103	✘	✘	✘	✘	✘	✔	✘	✔	✔	✔	✘	✘	✘	✘	✘
Tyr 91	HLA-DR2β Ile67	✘	✘	✘	✘	✘	✔	✔	✔	✔	✔	✘	✘	✘	✘	✘
Tyr 91	TCR-Vβ Thr100	✘	✘	✘	✘	✘	✔	✘	✔	✘	✘	✘	✘	✘	✘	✘
Asn 92	HLA-DR2α Asp66	✘	✘	✔	✔	✔	✘	✘	✘	✘	✘	✘	✘	✘	✘	✘

Table 4 continued

Residues		Interactions														
$MBP_{83–99}$ (Tyr^{91})	Receptor	Hydrogen bonds					Hydrophobic					Electrostatic				
		Conformers					Conformers					Conformers				
		1	2	3	4	5	1	2	3	4	5	1	2	3	4	5
Asn 92	HLA-DR2α Glu11	✔	✘	✔	✔	✔	✘	✘	✘	✘	✘	✘	✘	✘	✘	✘
Asn 92	HLA-DR2α Asn62	✘	✔	✘	✘	✘	✘	✘	✘	✘	✘	✘	✘	✘	✘	✘
Ile 93	HLA-DR2β Tyr30	✔	✘	✘	✘	✘	✔	✘	✘	✘	✘	✘	✘	✘	✘	✘
Ile 93	HLA-DR2α Asn69	✔	✔	✔	✔	✔	✘	✘	✘	✘	✘	✘	✘	✘	✘	✘
Ile 93	HLA-DR2β Trp61	✘	✘	✘	✘	✘	✔	✔	✔	✔	✔	✘	✘	✘	✘	✘
Ile 93	HLA-DR2β Ile67	✘	✘	✘	✘	✘	✔	✔	✔	✔	✔	✘	✘	✘	✘	✘
Ile 93	HLA-DR2β Tyr60	✘	✘	✘	✘	✘	✘	✔	✘	✘	✘	✘	✘	✘	✘	✘
Val 94	HLA-DR2β Trp61	✔	✘	✘	✘	✘	✘	✘	✘	✘	✘	✘	✘	✘	✘	✘
Val 94	HLA-DR2α Val65	✘	✘	✘	✘	✘	✔	✔	✔	✔	✔	✘	✘	✘	✘	✘
Val 94	HLA-DR2α Ala68	✘	✘	✘	✘	✘	✔	✔	✘	✔	✔	✘	✘	✘	✘	✘
Val 94	HLA-DR2α Ile72	✘	✘	✘	✘	✘	✔	✔	✘	✔	✘	✘	✘	✘	✘	✘
Val 94	HLA-DR2β Tyr60	✘	✘	✔	✘	✘	✘	✘	✘	✘	✘	✘	✘	✘	✘	✘
Thr 95	HLA-DR2α Asn69	✔	✘	✔	✔	✔	✘	✘	✘	✘	✘	✘	✘	✘	✘	✘
Thr 95	HLA-DR2β Asp57	✘	✔	✘	✔	✘	✘	✘	✘	✘	✘	✘	✘	✘	✘	✘
Thr 95	HLA-DR2α Ile72	✘	✘	✘	✘	✘	✔	✔	✔	✔	✔	✘	✘	✘	✘	✘
Thr 95	HLA-DR2α Met73	✘	✘	✘	✘	✘	✔	✔	✔	✔	✔	✘	✘	✘	✘	✘
Thr 95	HLA-DR2β Trp61	✘	✘	✘	✘	✘	✘	✔	✔	✔	✔	✘	✘	✘	✘	✘
Thr 95	HLA-DR2β Tyr60	✘	✘	✘	✘	✘	✘	✘	✔	✘	✘	✘	✘	✘	✘	✘
Pro 96	HLA-DR2β Tyr60	✘	✘	✘	✘	✘	✘	✔	✔	✔	✘	✘	✘	✘	✘	✘
Thr 98	HLA-DR2α Ile72	✘	✘	✘	✘	✘	✔	✘	✘	✘	✘	✘	✘	✘	✘	✘
Pro 99	HLA-DR2α Arg76	✘	✘	✔	✘	✔	✘	✘	✘	✘	✘	✘	✘	✘	✘	✔

The two chains of HLA-DR2 are denoted with α and β, and of TCR with Vα and Vβ

with Gln^{70} of HLA-DR2β. The hydrogen bonds mentioned above are stable during MD simulation with high occurrence (Table 6).

Furthermore, the peptide $MBP_{83–99}$ (Phe^{91}) is stabilized in the HLA-DR2 pocket with the following interactions: hydrogen bonds between Pro^{85}–Ser^{53} of HLA-DR2α, His^{88}–Asn^{82} of HLA-DR2α, electrostatic interactions between His^{88}–His^{81} of HLA-DR2α, hydrophobic interactions between Phe^{89}–Phe^{54} of HLA-DR2α, hydrogen bonds between Asn^{92}–Asp^{66} of HLA-DR2α, Asn^{92}–Trp^{61} of HLA-DR2β, and Ile^{93}–Tyr^{60} of HLA-DR2β, hydrophobic interactions between Asn^{92}–Asp^{66} of HLA-DR2α and Ile^{93}–Ile^{67} of HLA-DR2β, hydrogen bonding between Val^{94}–Tyr^{60} of HLA-DR2β, hydrophobic interactions between Val^{94}–Val^{65}, Ala^{68} and Ile^{72} of HLA-DR2α, hydrogen bonds between Thr^{95}–Asn^{69} of HLA-DR2α and Asp^{57} of HLA-DR2β, hydrophobic interactions between Thr^{95}–Ile^{72} and Met^{73} of HLA-DR2α and Trp^{61} of HLA-DR2β, between Pro^{96}–Tyr^{60} of HLA-DR2β, hydrogen bonding between Thr^{98}–Arg^{76} of HLA-DR2α and an electrostatic interaction between Pro^{99}–Lys^{75} of HLA-DR2α.

The peptide $MBP_{83–99}$ (Phe^{91}) forms also further interactions with TCR: hydrogen bonds between Glu^{83}–Glu^{59} of TCR-Vβ and Thr^{97} of TCR-Vα, Asn^{84}–Ala^{52} of TCR-Vα and electrostatic interactions between His^{88}–Asn^{104} of TCR-Vβ. Finally, there is also a combination of hydrogen bonding and electrostatic interactions between Glu^{83} and Lys^{99} of TCR-Vα.

A visualization of the binding pocket's hydrophilicity surface for the most favored conformer 3 of the peptide $MBP_{83–99}$ (Phe^{91}) in the trimolecular complex is presented in Fig. 4a. From the superimposition of the five most favored conformers of $MBP_{83–99}$ (Phe^{91}) produced by MD simulations (Fig. 4b), it is evident that linear and extended structures are the major characteristics of the low energy conformers situated in the binding site of the trimolecular complex.

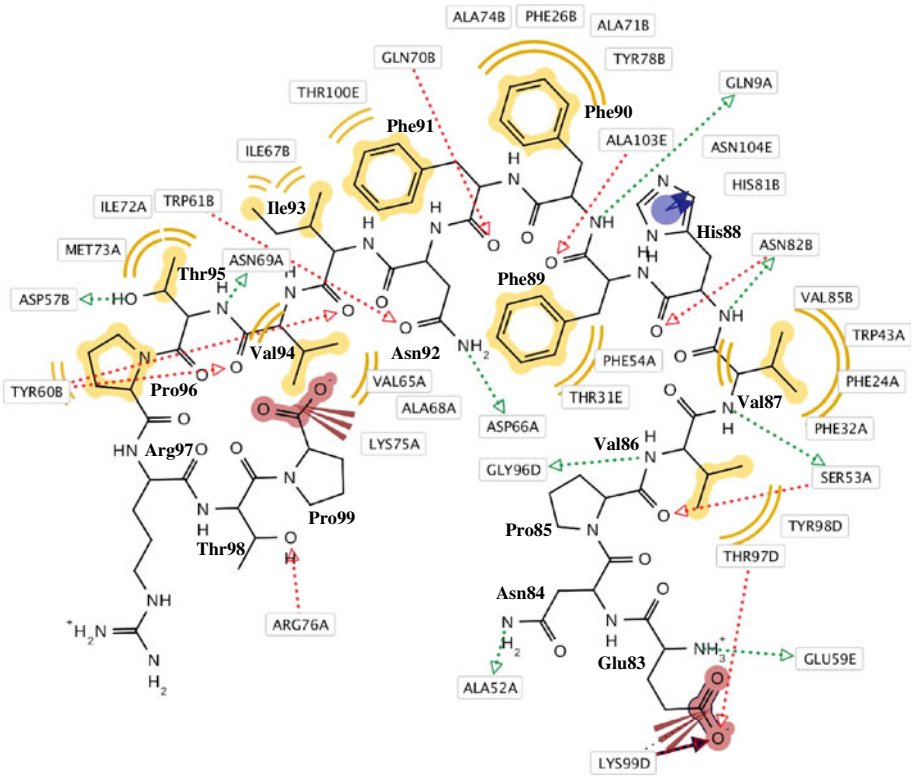

Fig. 3 Hydrogen bonds (donors *green*, acceptors *red*), hydrophobic interactions (*yellow*) and electrostatic interactions (*red* negative charged groups, *blue* positive charged groups) of the most favored conformation (3) of $MBP_{83–99}$ (Phe^{91}) during binding with amino acids of the receptor HLA-DR2 and TCR as they are revealed from the application of MD. The *letters* that accompany each amino acid correspond to the following: A = HLA-DR2α, B = HLA-DR2β, D = TCR-Vα and E = TCR-Vβ

MD results for the peptide $MBP_{83–99}$ (Tyr^{91})

The hydrogen bonding, the hydrophobic and electrostatic interactions of the most energetically favored conformer 3 of the peptide $MBP_{83–99}$ (Tyr^{91}) during binding with amino acids of the receptor HLA-DR2 and TCR are revealed from the application of MD in Fig. 5.

More specifically, the amino acid Val^{87} forms hydrogen bonding with Ser^{53} and Glu^{55} of HLA-DR2α and interacts through hydrophobic interactions with Phe^{24}, Ala^{52} and Phe^{54} of HLA-DR2α and with Val^{85} of HLA-DR2β. Phe^{90}, the other crucial amino acid for the binding to HLA-DR2, develops hydrogen bonding with Gln^{9} of HLA-DR2α and hydrophobic interactions with Phe^{26}, Ala^{71}, Tyr^{78} and Ala^{74} of HLA-DR2β.

The required interactions that are appearing during the recognition of $MBP_{83–99}$ (Tyr^{91}) with TCR are: hydrogen bonds between Phe^{89}–Ala^{103} of TCR-Vβ and Val^{86}–Gly^{96} of TCR-Vα, hydrophobic interaction between Val^{86}–Thr^{97} and Tyr^{98} of TCR-Vα, Val^{86}–Tyr^{58} of TCR-Vβ and between Phe^{89}–Thr^{31} of TCR-Vβ. The mutated amino acid Tyr^{91} forms hydrophobic interactions with Ile^{67} of HLA-DR2β and with Thr^{100} of TCR-Vβ. The mentioned hydrogen bonds are stable during MD simulation as indicated by their high occurrence (Table 6).

Further interactions which stabilize the peptide $MBP_{83–99}$ (Tyr^{91}) in the HLA-DR2 pocket are: hydrogen bonds between Pro^{85}–Ser^{53} of HLA-DR2α and His^{88}–Asn^{82} of HLA-DR2α, hydrophobic interactions between Pro^{85}–Val^{85} of HLA-DR2β, hydrogen bonds between Asn^{92}–Glu^{11} and Asp^{66} of HLA-DR2α and between Ile^{93}–Asn^{69} of HLA-DR2α, hydrophobic interactions between Ile^{93}–Trp^{61} and Ile^{67} of HLA-DR2β, hydrogen bond between Val^{94}–Tyr^{60} of HLA-DR2β, hydrophobic interactions between Val^{94}–Val^{65} of HLA-DR2α, hydrogen bonding between Thr^{95}–Asn^{69} of HLA-DR2α, hydrophobic interactions between Thr^{95}–Ile^{72} and Met^{73} of HLA-DR2α, Thr^{95}–Tyr^{60} and Trp^{61} of HLA-DR2β and between Pro^{96}–Tyr^{60} of HLA-DR2β and hydrogen bond between Pro^{99}–Arg^{76} of HLA-DR2α.

$MBP_{83–99}$ (Tyr^{91}) forms also the following interactions with the TCR: hydrogen bonds between Glu^{83}–Tyr^{58} and Gly^{61} of TCR-Vβ, between Asn^{84}–Tyr^{58} and Glu^{59} of TCR-Vβ, hydrophobic interactions between Pro^{85}–Thr^{97} of TCR-Vα and between Phe^{90}–Ala^{103} of TCR-Vβ.

The hydrophilicity surface of binding pocket for the most favored conformer 3 of the peptide $MBP_{83–99}$ (Tyr^{91}) in the trimolecular complex is shown in Fig. 6a. From the superimposition of the five most favored conformers of $MBP_{83–99}$ (Tyr^{91}) derived from MD simulations (Fig. 6b), it is obvious, also in this case, that linear and extended conformations are the major characteristics of $MBP_{83–99}$ (Tyr^{91}) low energy conformers situated in the binding site of the trimolecular complex.

Regarding the mutation of Lys^{91} $MBP_{83–99}$ with the amino acid Tyr^{91}, as in the case of Phe^{91}, it causes the abolishment of the α-helix formation observed between

Table 5 Comparison of hydrogen bonds, hydrophobic and electrostatic interactions of the two lowest energy conformers of the peptides $MBP_{83–99}$ (Phe^{91}) (conformer 3) and $MBP_{83–99}$ (Tyr^{91}) (conformer 3) and the proteins HLA-DR2 and TCR of the trimolecular complex

Peptide	Receptor	Conformers	
		$MBP_{83–99}$ (Phe^{91}) Conformer 3	$MBP_{83–99}$ (Tyr^{91}) Conformer 3
Hydrogen bonds			
Glu 83	TCR-Vα Lys99	✔	✘
Glu 83	TCR-Vβ Tyr58	✘	✔
Glu 83	TCR-Vβ Glu59	✔	✘
Glu 83	TCR-Vβ Gly61	✘	✔
Glu 83	TCR-Vα Thr97	✔	✘
Asn 84	TCR-Vβ Tyr58	✘	✔
Asn 84	TCR-Vβ Glu59	✘	✔
Asn 84	TCR-Vα Ala52	✔	✘
Pro 85	HLA-DR2α Ser53	✔	✔
Val 86	TCR-Vα Gly96	✔	✔
Val 87	HLA-DR2α Ser53	✔	✔
Val 87	HLA-DR2α Glu55	✘	✔
His 88	HLA-DR2β Asn82	✔	✔
Phe 89	TCR-Vβ Ala103	✔	✔
Phe 90	HLA-DR2α Gln9	✔	✔
Phe 91	HLA-DR2β Gln70	✔	–
Asn 92	HLA-DR2α Asp66	✔	✔
Asn 92	HLA-DR2β Trp61	✔	✘
Asn 92	HLA-DR2α Glu11	✘	✔
Ile 93	HLA-DR2β Tyr60	✔	✘
Ile 93	HLA-DR2α Asn69	✘	✔
Val 94	HLA-DR2β Tyr60	✔	✔
Thr 95	HLA-DR2α Asn69	✔	✔
Thr 95	HLA-DR2β Asp57	✔	✘
Thr 98	HLA-DR2α Arg76	✔	✘
Pro 99	HLA-DR2α Arg76	✘	✔
Hydrophobic interactions			
Pro 85	HLA-DR2β Val85	✘	✔
Pro 85	TCR-Vα Thr97	✘	✔
Val 86	TCR-Vβ Tyr58	✘	✔
Val 86	TCR-Vα Thr97	✔	✔
Val 86	TCR-Vα Tyr98	✔	✔
Val 87	HLA-DR2β Val85	✔	✔
Val 87	HLA-DR2α Phe32	✔	✘
Val 87	HLA-DR2α Trp43	✔	✘
Val 87	HLA-DR2α Ala52	✘	✔
Val 87	HLA-DR2α Phe54	✔	✔
Val 87	HLA-DR2α Phe24	✔	✔
Phe 89	TCR-Vβ Thr31	✔	✔
Phe 89	HLA-DR2α Phe54	✔	✘
Phe 90	HLA-DR2β Ala71	✔	✔
Phe 90	HLA-DR2β Phe26	✔	✔
Phe 90	HLA-DR2β Tyr 78	✔	✔
Phe 90	HLA-DR2β Ala74	✔	✔
Phe 90	TCR-Vβ Ala103	✘	✔
Phe 91	TCR-Vβ Thr100	✔	–
Tyr 91	TCR-Vβ Thr100	–	✔
Tyr 91	HLA-DR2β Ile67	–	✔
Asn 92	HLA-DR2α Asp66	✔	✘
Asn 92	HLA-DR2α Glu11	✘	✘
Ile 93	HLA-DR2β Trp61	✘	✔
Ile 93	HLA-DR2β Ile67	✔	✔
Val 94	HLA-DR2α Val65	✔	✔
Val 94	HLA-DR2α Ala68	✔	✘
Val 94	HLA-DR2α Ile72	✔	✘
Thr 95	HLA-DR2α Ile72	✔	✔
Thr 95	HLA-DR2α Met73	✔	✔
Thr 95	HLA-DR2β Trp61	✔	✔
Thr 95	HLA-DR2β Tyr60	✘	✔
Pro 96	HLA-DR2β Tyr60	✔	✔
Electrostatic interactions			
Glu 83	TCR-Vα Lys99	✔	✘
His 88	HLA-DR2β His81	✔	✘
His 88	TCR-Vβ Asn104	✔	✘
Pro 99	HLA-DR2α Lys75	✔	✘

The two chains of HLA-DR2 are denoted with α and β, and of TCR with Vα and Vβ

Table 6 Hydrogen bond interactions between specific residues responsible for the binding to HLA-DR2 and recognition of TCR of $MBP_{83–99}$ (Phe^{91}) and $MBP_{83–99}$ (Tyr^{91}) through the MD simulations

Hydrogen bond interaction		Occurrence (%)	
Peptide	HLA-TCR complex	$MBP_{83–99}$ (Phe^{91})	$MBP_{83–99}$ (Tyr^{91})
Val 86	TCR-Vα Gly96	85	75
Val 87	HLA-DR2α Ser53	77	90
Val 87	HLA-DR2α Glu 55	0	76
Phe 89	TCR-Vβ Ala103	92	95
Phe 90	HLA-DR2α Gln9	100	100
Phe 90	HLA-DR2α Asn62	81	77
Phe 91	HLA-DR2β Gln70	100	–
Asn 92	HLA-DR2α Asp66	97	82
Asn 92	HLA-DR2β Trp 61	67	0
Asn 92	HLA-DR2α Glu11	1	83
Ile 93	HLA-DR2β Tyr60	67	1
Ile 93	HLA-DR2α Asn69	7	86

The hydrogen bond interactions of other neighboring residues of mutation site 91 are included

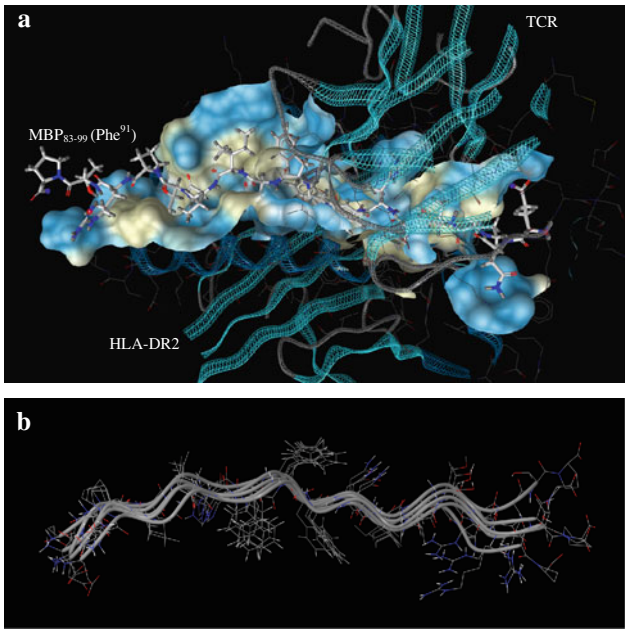

Fig. 4 **a** The most favored conformer (3) of $MBP_{83–99}$ (Phe^{91}) in the trimolecular complex along with the hydrophilicity surface of the binding pocket (*blue* and *white colors* represent the hydrophilic and the hydrophobic areas, respectively). **b** Superimposition of the 5 conformers of $MBP_{83–99}$ (Phe^{91}) derived from the MD

amino acids Val^{87}–Phe^{90} [13, 35]. As far as the interactions of $MBP_{83–99}$ (Tyr^{91}) for the TCR recognition, His^{88} is not involved, as in the $MBP_{83–99}$ (Phe^{91}) case.

Comparative binding motif study between $MBP_{83–99}$ (Phe^{91}) and $MBP_{83–99}$ (Tyr^{91})

The two linear and extended peptides showed similarities and differences concerning their binding motif to the receptor. Comparison of the most important interactions of the two peptides on the receptor HLA-DR2 is shown in Table 5. Peptide $MBP_{83–99}$ (Phe^{91}) forms with the amino acids of the receptor HLA-DR2 and TCR more hydrogen bonds relatively to the $MBP_{83–99}$ (Tyr^{91}). As a representative example, is shown the lowest energy conformer 3 of $MBP_{83–99}$ (Phe^{91}) that forms 18 hydrogen bonds, in comparison to 17 of the corresponding lowest energy conformer 3 of the $MBP_{83–99}$ (Tyr^{91}). The number of hydrogen bonds per timeframe through the MD calculations is shown in Fig. 7. $MBP_{83–99}$ (Phe^{91}) has an average of hydrogen bonds of 15.2 over $MBP_{83–99}$ (Tyr^{91}) which has 12.7 hydrogen bonds per timeframe.

More details in a quantitative fashion of the principal hydrogen bond interactions between specific residues of $MBP_{83–99}$ (Phe^{91}), $MBP_{83–99}$ (Tyr^{91}) and HLA-TCR complex through the MD simulations are shown in Table 6. Both peptides have similar occupancy concerning hydrogen bonding network of residues Val^{86}, Phe^{89}, and Phe^{90} with HLA-TCR complex. The major differences are the hydrogen bond interaction between Val^{87}–Glu^{55} of HLA-DR2α of $MBP_{83–99}$ (Tyr^{91}), which is not observed for $MBP_{83–99}$ (Phe^{91}) and hydrogen bond interaction of mutated amino acid Phe^{91} with Gln^{70} of HLA-DR2α, while Tyr^{91} is lacking such a hydrogen bond.

RMSD calculation of $MBP_{83–99}$ (Phe^{91}) residues Val^{86}, Val^{87}, Phe^{89}, Phe^{90}, Phe^{91}, and HLA-TCR complex residues Gln^{9}, Ser^{53}, Asn^{62} (HLA-DR2α), Gln^{70} (HLA-DR2β), Gly^{96} (TCR-Vα), Ala^{103} (TCR-Vβ) that interact through important hydrogen bonds and respectively for $MBP_{83–99}$ (Tyr^{91}) residues Val^{86}, Val^{87}, Phe^{89}, Phe^{90} and HLA-TCR complex residues Gln^{9}, Ser^{53}, Glu^{55} (HLA-DR2α), Gly^{96} (TCR-Vα), Ala^{103} (TCR-Vβ) showed that this ranged between 0–0.05 Å through MD trajectory (results not shown).

More specifically, the most important similarities and differences are: Val^{87} and Phe^{90} of both peptides, responsible for the binding to HLA-DR2, share several common interactions with amino acids of the receptor. $MBP_{83–99}$ (Phe^{91}) appears to develop two additional hydrophobic interactions between Val^{87}–Phe^{32} and Trp^{43} of HLA-DR2α. However, Val^{87} of $MBP_{83–99}$ (Tyr^{91}) forms an additional stable hydrogen bond with Glu^{55} of HLA-DR2α and one additional hydrophobic interaction with Ala^{52} of HLA-DR2a (Table 5).

Val^{86} and Phe^{89}, crucial amino acids for the TCR recognition of both peptides, share common hydrogen bonding regarding Val^{86}–Gly^{96} of TCR-Vα, Phe^{89}–Ala^{103} of TCR-Vβ and hydrophobic interactions between Val^{86}–Thr^{97}, Tyr^{98} of TCR-Vα and Phe^{89}–Thr^{31} of TCR-Vβ. $MBP_{83–99}$ (Phe^{91}) lacks the hydrophobic interaction between Val^{86}–Tyr^{58} of TCR-Vβ, which is present in the case of $MBP_{83–99}$ (Tyr^{91}) (Table 5).

Phe^{91} of the peptide $MBP_{83–99}$ (Phe^{91}) interacts with both HLA-DR2 and TCR forming one stable hydrogen bonding with Gln^{70} of HLA-DR2β and hydrophobic interaction with Thr^{100} of TCR-Vβ. The corresponding amino acid Tyr^{91} of $MBP_{83–99}$ (Tyr^{91}) interacts with HLA-TCR complex only through hydrophobic interactions with Ile^{67} of HLA-DR2β and with Thr^{100} of TCR-Vβ. Moreover, only $MBP_{83–99}$ (Phe^{91}) forms electrostatic interactions with HLA-DR2 and TCR; between Glu^{83}–Lys^{99} of TCR-Vα, His^{88}–His^{81} of HLA-DR2β and Asn^{104} of TCR-Vβ, and Pro^{99}–Lys^{75} of HLA-DR2α (Table 5).

The mutation at position 91 affects also the conformation and interactions of neighboring residues, especially of Asn^{92} and Ile^{93} (Figs. 3, 6 and 8). More specifically, the Asn^{92} of $MBP_{83–99}$ (Phe^{91}) develops hydrogen bonds with Asp^{66} of HLA-DR2α and Trp^{61} of HLA-DR2β while in the case of $MBP_{83–99}$ (Tyr^{91}) it interacts with Asp^{66} and Glu^{11} of HLA-DR2α. Regarding the Ile^{93} of $MBP_{83–99}$ (Phe^{91}) forms hydrogen bonding with Tyr^{60} of HLA-DR2β and hydrophobic interactions with Ile^{67} of HLA-DR2β, but in

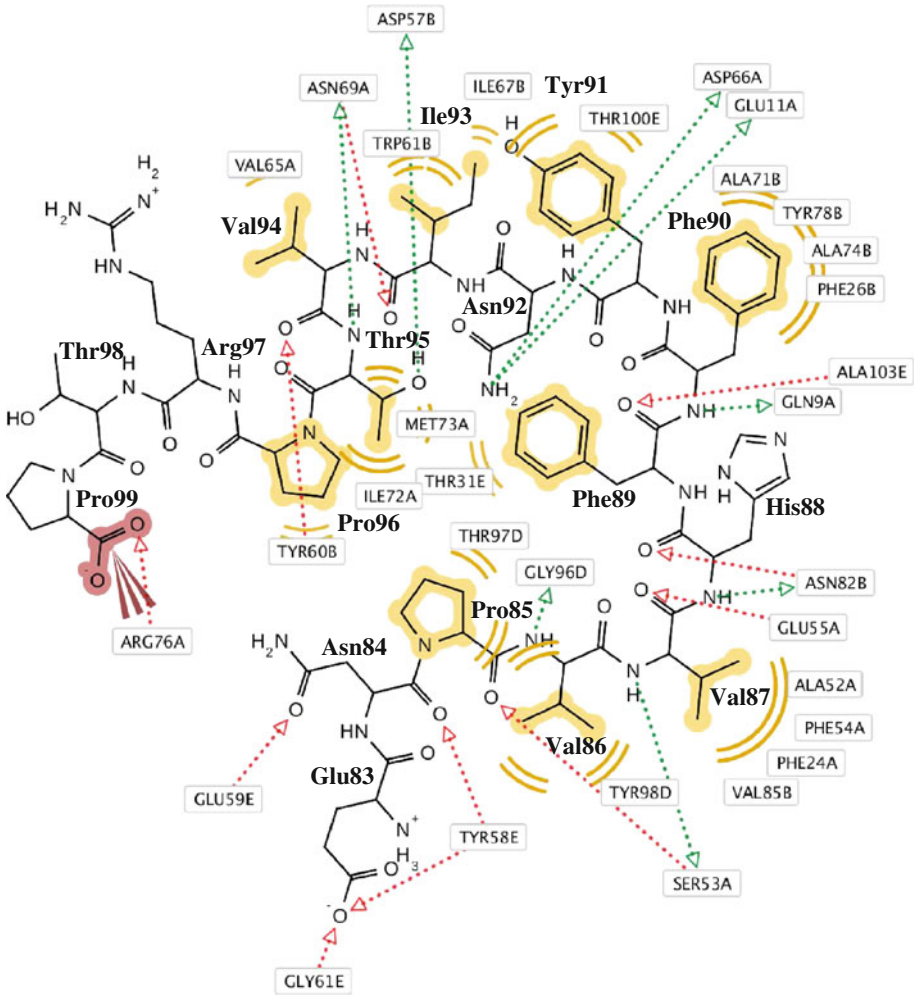

Fig. 5 Hydrogen bonds (donors *green*, acceptors *red*), hydrophobic interactions (*yellow*) and electrostatic interactions (*red* negative charged groups, *blue* positive charged groups) of the most favored conformer (3) of $MBP_{83–99}$ (Tyr^{91}) during binding with amino acids of the receptor HLA-DR2 and TCR as they are revealed from the application of MD. The *letters* that accompany each amino acid correspond to the following: A = HLA-DR2α, B = HLA-DR2β, D = TCR-Vα and E = TCR-Vβ

the case of $MBP_{83–99}$ (Tyr^{91}) Ile^{93} forms hydrogen bond with Asn^{69} of HLA-DR2α and hydrophobic interaction not only with Ile^{67} of HLA-DR2β but also with Trp^{61} of HLA-DR2β. All the above described hydrogen bonds are stable through the MD simulations (Table 6).

When another strategy was used, more specifically, when MD simulation was applied using the mutated crystal structure of $MBP_{83–96}$ at position 91 and extended until position 99, identical results were obtained. Although, this strategy is simpler, we find our above mentioned approach more general in terms of simulating the system for the following reasons: (a) We proved that synthetic peptides accommodate in the same place as the wild peptide; (b) Low energy conformers of the synthetic peptides are in accordance with NMR results; (c) We explored, through docking, the conformational preferences of the elongated, regarding to the wild type, peptides (d) The applied extended MD calculations allow the exploration of the mobility of the system; (e) Our approach expands the conformational space for the ligand as it combines the use of experimental NMR and theoretical results (combination of docking and MD calculations).

Conclusion

The two peptides under study show similarities and differences in respect to their binding motif with HLA-DR2 and TCR receptors. In general, $MBP_{83–99}$ (Phe^{91}) shows more interactions at the formation of the trimolecular complex compared to $MBP_{83–99}$ (Tyr^{91}), concerning the comparison of hydrogen bond occupancy over MD trajectories, as well as the comparison of all interactions of the most energetically favored conformers. The better biological profile of the latter may be due to this reason, thus its distinct number of interactions may be responsible to reduce the immunological response through the activation of encephalitogenic T-cells and finally the appearance of MS.

The two molecules also show differences in the binding motif in comparison with the wild epitope $MBP_{83–96}$. This is attributed to the fact that by mutating Lys^{91} by either Tyr or Phe the stereoelectronic characteristics become different. This modification of the stereoelectronic properties can affect at least the binding motif of the regional amino acids. This may also explain their antagonistic versus agonistic

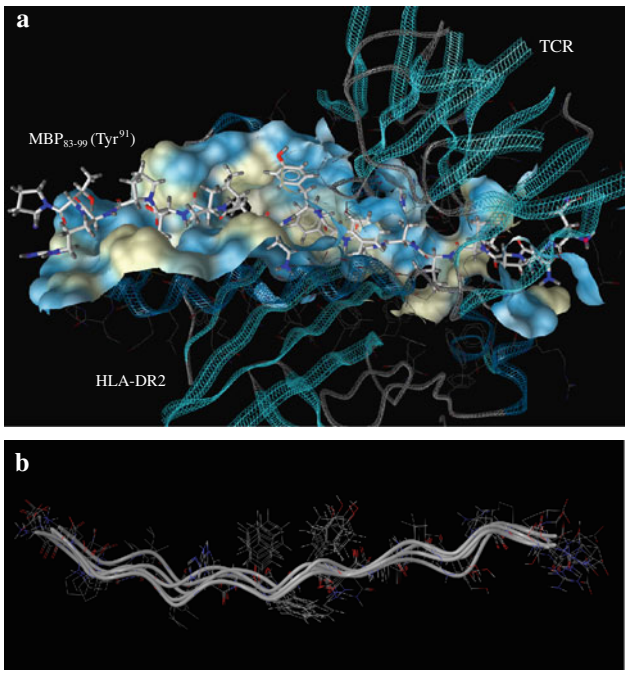

Fig. 6 **a** The most favored conformer (3) of $MBP_{83–99}$ (Tyr^{91}) in the trimolecular complex along with the hydrophilicity surface of the binding pocket (*blue* and *white colors* represent the hydrophilic and the hydrophobic areas, respectively). **b** Superimposition of the 5 conformers of $MBP_{83–99}$ (Tyr^{91}) derived from the MD

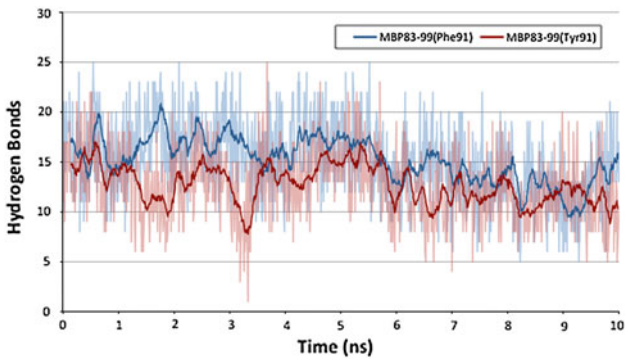

Fig. 7 Number of hydrogen bonds per timeframe through the MD simulations. In *dark blue* and *dark red*, a moving average has been calculated for clarification of the results

activity. Such differences in the binding motifs between linear and cyclic agonists and antagonists analogues of $MBP_{87–99}$ epitope were also shown in our previous work [19–26].

It has to be mentioned that although the two peptides studied differ only in a small segment, they have as it is mentioned above a distinct biological profile. More specifically, the tyrosine amino acid of $MBP_{83–99}$ (Tyr^{91}) possesses the phenolic group which is responsible for inducing different biological activity. This is not surprising

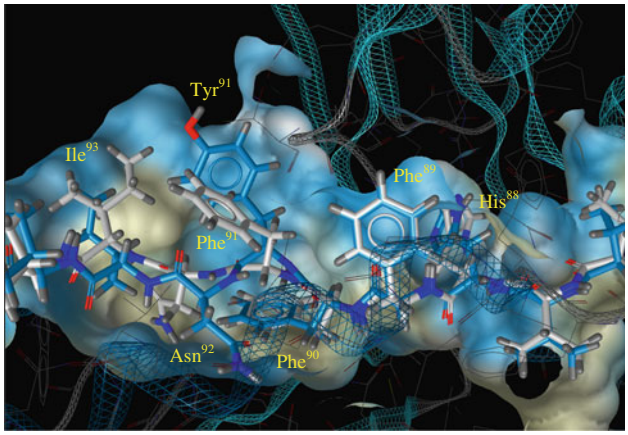

Fig. 8 Superimposition of the most favored conformer (3) of $MBP_{83–99}$ (Phe^{91}) (in *grey*) and the most favored conformer (3) of $MBP_{83–99}$ (Tyr^{91}) (in *blue*) at the binding site of the trimolecular complex, consisted of HLA-DR2, TCR and the peptide, along with the hydrophilicity surface of the binding pocket (*blue* and *white colors* represent the hydrophilic and the hydrophobic areas, respectively)

as it is well known from different classes of biological important molecules that phenolic group plays a pivotal role in drug bioactivity [36–47]. Thus, although the superimposition of the two peptides at the binding site of the trimolecular complex shows that the mutated amino acids Phe^{91} and Tyr^{91} occupy almost the same area, they induce different conformation to other amino acids such as Asn^{92} and Ile^{93} because the phenolic group is situated in a relatively hydrophobic environment. This differentiation affects the interactions of the neighboring residues of the two peptides. It is evident from our results that this small structural difference between the two peptides can lead to a cascade of distinct interactions that determine their fingerprint of biological profile.

More work is needed to reveal the subtle interactions that govern the bioactivity. Effort must be made to understand: (a) the forces that determine the folding of the epitope; (b) the conservation of the linearity and extended structure of the altered epitope; (c) the molecular features of the altered epitope that maximize the productive interactions with HLA-DR2 and minimize the contacts with TCR.

Materials and methods

Peptide synthesis and purification

2-chlorotrityl chloride resin (0.7–1.0 mmol Cl^{-}/g resin, 400 mesh), Fmoc-Pro-OH, Fmoc-Thr(tBu)-OH, Fmoc-Arg(Pbf)-OH, Fmoc-Val-OH, Fmoc-Ile-OH, Fmoc-Asn-OH, Fmoc-Tyr(tBu)-OH, Fmoc-Phe-OH and Fmoc-

His(Trt)-OH, Fmoc-Glu(tBu)-OH, were obtained from Chemical to Biopharmaceutical Laboratories of Patras, Patras, Greece. All solvents and other reagents were purchased from Merck, Sigma-Aldrich and Fluka chemical companies. DC-Alufolien Kieselgel 60 (Merck) was used for Thin Layer Chromatography (TLC) analysis of synthetic products with the following eluent solvent: *n*-butanol/acetic acid/water (BAW) 4:1:1 (v/v/v). Peptides were purified by semi-preparative Reverse Phase High Performance Liquid Chromatography (RP-HPLC) on a Waters system equipped with a 600E controller and a Waters 996 photodiode array UV detector. The analysis was controlled by an Millenium 2.1 operating system and a Nucleosil C-18 reversed phase analytical column (250 × 10 mm with 7 μm packing material). Electron Spray Ionization Mass Spectroscopy (ESI–MS) experiments were performed on a TSQ 7000 spectrometer (Electrospray Platform LC of Micromass) coupled to a MassLynx NT 2.3 data system. The purity of the two compounds was found to be ≥95%.

Synthesis of $MBP_{83–99}$ (Phe^{91}) and $MBP_{83–99}$ (Tyr^{91}) peptide analogues

The linear peptides were prepared on 2-chlorotrityl chloride resin (CLTR-Cl) using the Fmoc/tBu solid-phase methodology [28–31]. The first N^{α} Fmoc (9-fluorenylmethyloxycarboxyl)-protected amino acid (Fmoc-Pro-OH) was esterified to the resin in the presence of diisopropylethylamine (DIPEA) in dichloromethane (DCM) in 1 h at RT [28–31]. DCM/MeOH/DIPEA (85:10:5) was then added and the resulting mixture was stirred for another 10 min at RT. The remaining protected peptide chains were assembled by sequential couplings of the appropriate Fmoc protected amino acids (2.5 equiv), in the presence of *N,N'*-diisopropylcarbodiimide (DIC) (2.75 equiv) and 1-hydroxybenzotriazole (HOBt) (3.75 equiv) in *N,N*-dimethylformamide (DMF) [28–31]. The completeness of each coupling was verified by the Kaiser test and TLC using a BAW, 4:1:1 (v/v/v) eluent system and the Fmoc protecting group was removed by treatment with piperidine solution (20% in DMF). The synthesized protected peptide on the resin was then cleaved with the splitting solution dichloromethane/2,2,2-trifluoroethanol (DCM/TFE, 7/3, 2 h at RT). The mixtures were filtered, the solvents were removed on a rotary evaporator and the obtained oily products were precipitated from cold dry diethyl ether as white solids. The linear protected peptides were treated with 70% TFA in DCM in the presence of 0.3% 1,2-ethanedithiol, anisole and H_2O as scavengers for 5 h at RT. The purification of each peptide was carried out using semi-preparative RP-HPLC and peptide purity was assessed by analytical RP-HPLC (column: Nucleosil C18, 5 μm, 4.6 × 250 mm). They were identified by ESI–MS.

NMR spectroscopy

The high-resolution NMR spectra were recorded on a Varian DirectDrive 800 MHz spectrometer at 25 °C. 2 mg of each peptide were dissolved in 0.7 ml of DMSO-d_6. The 2D TOCSY [48] and 2D NOESY [49] experiments were recorded using the standard pulse sequences in the phase-sensitive mode. The 2D homonuclear proton spectra were acquired with a spectral width of 8,012 Hz, 2,048–4,096 data points in t_2, 4–32 scans, 512 complex points in t_1, and a relaxation delay of 1.5 s. The mixing times in 2D NOESY and 2D TOCSY experiments were 75 ms and 60 ms, respectively. The $^{1}H–^{13}C$ HSQC was performed with gradients and was recorded with 32 scans and 128 complex points in t_1, ^{1}H spectral width of 8,013 Hz, ^{13}C spectral width of 30,166 Hz, 512 data points in t_2 and a relaxation delay of 1 s.

The data was processed and analyzed with Mnova software from Mestrelab Research. Crosspeak volumes in NOESY spectra were calculated by integration routine within the Mnova software. A set of strong (up to 2.5 Å), medium (2.5–3.7 Å), and weak (3.7–5 Å) NOEs was established according to the integrated intensity of the geminal pair of protons $\gamma 1$ and $\gamma 2$ of Ile^{93}, which have a distance of 1.78 Å in all conformations.

Molecular modeling

The extended crystal structure of $MBP_{83–96}$ (pdb code: 1YMM) was mutated at amino acid 91 with either Phe^{91} or Tyr^{91} and extended with amino acid residues 87–89 to provide peptides $MBP_{83–99}$ (Phe^{91}) and $MBP_{83–99}$ (Tyr^{91}). The resulting structures were optimized using the Steepest Descent and Truncated Newton Conjugate Gradient (TNCG) minimization algorithms. The optimized structures were in accordance to the observation of strong sequential $d_{\alpha N(i,i+1)}$ NOE connectivities and the absence of long range NOEs. The two peptides under study were then docked in the pocket of the native peptide $MBP_{83–96}$. During docking the peptides were held flexible.

All docking simulations were performed on Discovery Studio 2.0 by Accelrys Software Inc [50] with the LigandFit method, on the Dreiding Energy Grid force field [51] using the experimental crystal structure coordinates of the major histocompatibility complex bonded to a human autoimmune T cell receptor (pdb code: 1ymm) [34]. The co-crystallized peptide of $MBP_{83–96}$ as well as water molecules were removed. This approach was performed in order to dock and obtain the optimal peptide–receptor complexes in terms of binding affinity for the two molecules, $MBP_{83–99}$ (Phe^{91}) and $MBP_{83–99}$ (Tyr^{91}). The docking experiments resulted on various docked conformations, for both molecules. Performing the LigandScore function, top dock scoring conformations for each peptide

were extracted to be further examined on their stability through Molecular Dynamics runs.

The best docking poses for each peptide were subjected to Molecular Dynamics (MD). A total of 1,000 conformers from the trajectory file were divided into 5 families according to their RMSD values based on heavy atoms. The trimolecular complexes for the lowest energy conformer from each cluster were subjected to Truncated Newton Conjugate Gradient (TNCG) minimization.

Molecular Dynamics simulations were performed on the GROMACS 4.5.3 software package [52] using the GROMOS96 force field [53]. The best docked conformations of the peptides $MBP_{83–99}$ (Phe^{91}) and $MBP_{83–99}$ (Tyr^{91}) were subjected to Molecular Dynamics simulations where in each case, the system included the peptide, the major histocompatibility complex, the human autoimmune T cell receptor and ~66,000 water molecules in a cubic box with dimensions 110 × 180 × 110 (Å). Simulations were run at 300 K using the Berendsen pressure coupling method and electrostatic interactions were calculated using the particle mesh Ewald method [54]. Cutoff distances for the calculation of Coulomb and van der Waals interactions were 1.0 and 1.4 nm, respectively. Prior to the Molecular Dynamics simulations, energy minimization was applied to the full system without constraints using the Steepest Descent integrator for 1,000 steps with a time step of 2 fs (the minimization tolerance was set to 1,000 kJ/(mol.nm)). The systems were then equilibrated via 300 ps simulations with a time step of 2 fs. Finally, a 10 ns production run was performed for the systems, respectively, at 300 K with a time step of 2 fs using the Berendsen thermostat algorithm as all bonds were constrained using the LINCS algorithm [55]. Visualization of the dynamics trajectories was performed with the VMD software package [56].

The clustering of the selected 1,000 conformers of the peptides was performed by Cheminformatics/Canvas [57] module of Schrodinger Suite 2010 followed by energy minimization using Truncated Newton Conjugate Gradient (TNCG) algorithm of Macromodel module on Maestro platform of Schrodinger Suite 2010 [58].

LigandScout 3.0 (evaluation version) was used for the visualization of the interactions of the peptides at the binding site of the trimolecular complex. Hydrogen bonding default angle ranges are used (donor: sp^2 below 50°, sp^3 below 34°, acceptor: below 85°). For hydrophobic interactions also default threshold values were used (rings 0.6 Å, chains 1.0 Å, groups 0.47 Å and the surface accessibility threshold was set 0.25 Å [59].

Acknowledgments This work was partially supported by EN-FIST Centre of Excellence (Dunajska 156, SI-1000 Ljubljana, Slovenia) and Ministry of Higher Education, Science and Technology of Slovenia. We acknowledge A. Suarez amd M. Mavromoustakos for their linguistic amendment of the manuscript. We gratefully thank Prof. Leonardo Pardo (Universitat Autónoma de Barcelona) for computer facilities and software use.

References

1. Kenealy SJ, Perical-Vance MA, Haines JL (2003) The genetic epidemiology of MS. J Neuroimmunol 143:7–12
2. Prat E, Martin R (2002) The immunopathogenesis of MS. J Rehabil Res Dev 39:187–200
3. Aguado B, Bahram S, Beck S, Campbell RD, Forbes SA, Geraghty D, Guillaudeux T, Hood L, Horton R, Inoko H, Janer M, Jasoni C, Madan A, Milne S, Neville M, Oka A, Qin S, Ribas-Despuig G, Rogers J, Rowen L, Shiina T, Spies T, Tamiya G, Tashiro H, Trowsdale J, Vu Q, Williams L, Yamazaki M, Sequence Consortium MHC (1999) Complete sequence and gene map of a human MHC complex. Nature 401:921–923
4. Compston A, Coles A (2002) Multiple sclerosis. Lancet 359:1221
5. Barcellos LF, Thomson G (2003) Genetic analysis of MS. J Neuroimmunol 143:1–6
6. Muraro PA, Vergelli M, Kalbus M, Banks DE, Nagle J, Tranquill LR, Nepom GT, Biddison WE, McFarland HF, Martin R (1997) Immunodominance of a low-affinity major histocompatibility complex-binding myelin basic protein epitope in HLADR4. J Clin Invest 100:339–349
7. Ota K, Matsui M, Milford EL, Mackin GA, Weiner HL, Hafler DA (1990) T-cell recognition of an immunodominant myelin basic protein epitope in multiple sclerosis. Nature 346: 183–187
8. Martin R, Howell MD, Jaraquemada D, Flerlage M, Richert J, Brostoff S, Long EO, McFarlin DE, McFarland HF (1991) A myelin basic protein peptide is recognized by cytotoxic T cells in a context of four HLA-DR types associated with multiple sclerosis. J Exp Med 173:19–24
9. Zhang J, Markovic-Plese S, Lacet B, Raus J, Weiner HL, Hafler DA (1994) Increased frequency of interleukin 2-responsive T cells specific for myelin basic protein and proteolipid protein in peripheral blood and cerebrospinal fluid of patients with multiple sclerosis. J Exp Med 179:973–984
10. Zamvil SS, Steinman L (1990) The T lymphocyte in experimental allergic encephalomyelitis. Annu Rev Immunol 8:579–621
11. Valli A, Sette A, Kappos L, Oseroff C, Sidney J, Miescher G, Hochberger M, Albert ED, Adorini L (1993) Binding of myelin basic protein peptides to human histocompatibility leukocyte antigen class II molecules and their recognition by T cells from multiple sclerosis patients. J Clin Invest 91:616–628
12. Kalbus M, Fleckenstein BT, Offenhausser M, Bluggel M, Melms A, Meyer HF, Rammensee HG, Martin R, Jung G, Sommer N (2001) Ligand motif of the autoimmune disease-associated mouse MHC class II molecule H2-A(s). Eur J Immunol 31:551–562
13. Spyranti Z, Tselios T, Deraos G, Matsoukas J, Spyroulias GA (2010) NMR structural elucidation of myelin basic protein epitope 83–99 implicated in multiple sclerosis. Amino Acids 38:929–936
14. Bielekova B, Goodwin B, Richert N, Cortese I, Kondo T, Afshar G, Gran B, Eaton J, Antel J, Frank JA, McFarland HF, Martin R (2000) Encephalitogenic potential of the myelin basic protein peptide (amino acids 83–99) in multiple sclerosis: results of a phase II clinical trial with an altered peptide ligand. Nat Med 6:1167–1175
15. Kappos L, Comi G, Panitch H, Oger J, Antel J, Conlon P, Steinman L (2000) The altered peptide ligand in relapsing MS study NMR of MBP 83–99 epitope group. Induction of a non-encephalitogenic type 2 T helper-cell autoimmune response in multiple sclerosis after administration of an altered peptide ligand in a placebo-controlled, randomized phase II trial. Nat Med 6:1176–1182

16. Katsara M, Yuriev E, Ramsland PA, Deraos G, Tselios T, Matsoukas J, Apostolopoulos V (2008) A double mutation of MBP(83–99) peptide induces IL-4 responses and antagonizes IFN-gamma responses. J Neuroimmunol 200:77–89
17. Katsara M, Yuriev E, Ramsland PA, Deraos G, Tselios T, Matsoukas J, Apostolopoulos V (2008) Mannosylation of mutated MBP83–99 peptides diverts immune response from Th1 to Th2. Molec Immunol 45:3661–3670
18. Katsara M, Deraos G, Tselios T, Matsoukas J, Apostolopoulos V (2008) Design of novel cyclic altered peptide ligands of myelin basic protein MBP83–99 that modulate immune responses in SJL/J mice. J Med Chem 51:3971–3978
19. Pellecchia M, Bertini I, Cowburn D, Dalvit C, Giralt E, Jahnke W, James TL, Homans SW, Kessler H, Luchinat C, Meyer B, Oschkinat H, Peng J, Schwalbe H, Siegal G (2008) Perspectives on NMR in drug discovery: a technique comes of age. Nat Rev Drug Discov 7:738–745
20. Li X, Peterkofsky A, Wang G (2008) Solution structure of NPr, bacterial signal-transducing protein that controls the phosphorylation state of the potassium transporter-regulating protein IIANtr. Amino acids 35:531–539
21. Mantzourani ED, Mavromoustakos TM, Platts JA, Matsoukas JM, Tselios T (2005) Structural requirements for binding of myelin basic protein (MBP) peptides to MHC II: effects on immune regulation. Curr Med Chem 12:1521–1535
22. Mantzourani ED, Tselios TV, Grdadolnik SG, Platts JA, Brancale A, Deraos G, Matsoukas JM, Mavromoustakos TM (2006) Comparison of proposed putative active conformations of linear altered peptide ligands of myelin basic protein epitope 87–99 by spectroscopic and modelling studies: the role of position 91 and 96 in T-cell receptor activation. J Med Chem 49:6683–6691
23. Mantzourani ED, Tselios TV, Grdadolnik SG, Brancale A, Platts JA, Matsoukas JM, Mavromoustakos TM (2006) A putative bioactive conformation for the altered peptide ligand of myelin basic protein and inhibitor of experimental autoimmune encephalomyelitis [Arg91, Ala96] MBP87–99. J Mol Graph Mod 25:17–29
24. Mantzourani ED, Platts JA, Brancale A, Mavromoustakos TM, Tselios TV (2007) Molecular dynamics at the receptor level of immunodominant myelin basic protein epitope 87–99 implicated in multiple sclerosis and its antagonists altered peptide ligands: triggering of immune response. J Mol Graphics Model 26:471–481
25. Mantzourani E, Laimou D, Matsoukas MT, Tselios T (2008) Peptides as therapeutic agents or drug leads for autoimmune, hormone dependent and cardiovascular diseases. Anti-inflamm Anti-allergy Agents Med Chem 7:294–306
26. Mantzourani ED, Blokar K, Tselios TV, Matsoukas JM, Platts JA, Mavromoustakos TM, Grdadolnik SG (2008) A combined NMR and molecular dynamics simulation study to determine the conformational properties of agonists and antagonists against experimental autoimmune encephalomyelitis. Bioorg Med Chem 16:2171–2182
27. Spyranti Z, Dalkas GA, Spyroulias GA, Mantzourani ED, Mavromoustakos T, Friligou I, Matsoukas JM, Tselios TV (2007) Putative bioactive conformations of amide linked cyclic myelin basic protein peptide analogues associated with experimental autoimmune encephalomyelitis. J Med Chem 50:6039–6047
28. Tselios T, Probert L, Daliani I, Matsoukas E, Troganis A, Gerothanassis I, Mavromoustakos T, Moore G, Matsoukas J (1999) Design and synthesis of a potent cyclic analogue of the myelin basic protein epitope MBP72–85: importance of the Ala81 carboxyl group and of a cyclic conformation for induction of experimental allergic encephalomyelitis. J Med Chem 42:1170–1177
29. Tselios T, Daliani I, Deraos S, Thymianou S, Matsoukas E, Troganis A, Gerothanassis I, Mouzaki A, Mavromoustakos T, Probert L, Matsoukas J (2000) Treatment of experimental allergic encephalomyelitis (EAE) by a rationally designed cyclic analogue of myelin basic protein (MBP) epitope 72–85. Bioorg Med Chem Lett 10:2713–2717
30. Tselios T, Apostolopoulos V, Daliani I, Deraos S, Grdadolnik S, Mavromoustakos T, Melachrinou M, Thymianou S, Probert L, Mouzaki A, Matsoukas J (2002) Antagonistic effects of human cyclic MBP(87–99) altered peptide ligands in experimental allergic encephalomyelitis and human T-cell proliferation. J Med Chem 45:275–283
31. Tselios T, Daliani I, Deraos S, Thymianou S, Matsoukas E, Troganis A, Gerothanassis I, Mouzaki A, Mavromoustakos T, Probert L, Matsoukas J (2000) Treatment of experimental allergic encephalomyelitis (EAE) by a rationally designed cyclic analogue of myelin basic protein (MBP) epitope 72–85. Bioorg Med Chem Let 10:2713–2717
32. Soteriadou KP, Tzinia AK, Panou-Pamonis E, Tsikaris V, Sakarellos-Daitsiotis M, Sakarellos C, Papapoulou Y, Matsas R (1996) Antigenicity and conformational analysis of the Zn(2+)-binding sites of two Zn(2+)-metalloproteases: Leishmania gp63 and mammalian endopeptidase-24.11. Biochem J 313:455–466
33. LaPlanche LA, Rogers MT (1964) Cis and trans configurations of the peptide bond in N-monosubstituted amides by nuclear magnetic resonance. J Am Chem Soc 86:337–341
34. Hahn M, Nicholson MJ, Pyrdol J, Wucherpfennig KW (2005) Unconventional topology of self peptide-major histocompatibility complex binding by a human autoimmune T cell receptor. Nat Immunol 6:490–496
35. Fares C, Libich DS, Harauz G (2006) Solution NMR structure of an immunodominant epitope of myelin basic protein. FEBS J 273:601–614
36. Martel P, Makriyannis A, Mavromoustakos T, Kelly K, Jeffrey KR (1993) Topography of tetrahydrocannabinol in model membranes using neutron diffraction. Biochim Biophys Acta 1151:51–58
37. Mavromoustakos T, Daliani I (1999) Effects of cannabinoids in membrane bilayers containing cholesterol. Biochim Biophys Acta 1420:252–265
38. Mavromoustakos T, Theodoropoulou E (1998) A combined use of ^{13}C-cross polarization/magic angle spinning, ^{13}C-magic angle spinning and ^{31}P nuclear magnetic spectroscopy with differential scanning calorimetry to study cannabinoid-membrane interactions. Chem Phys Lipids 92:37–52
39. Mavromoustakos T, Yang DP, Broderick W, Fournier D, Herbette LG, Makriyannis A (1991) Small angle X-Ray diffraction studies on the topography of cannabinoids in synaptic plasma membranes. Pharmacol Biochem Behav 40:547–552
40. Mavromoustakos T, Yang D, Makriyannis A (1994) Topography of Alphaxalone and Δ16-alphaxalone in membrane bilayers containing cholesterol. Biochim Biophys Acta 1194:69–74
41. Mavromoustakos T, Yang DP, Makriyannis A (1995) Small angle x-ray diffraction and differential scanning calorimetric studies on O-methyl-(−)-Δ8-Tetrahydrocannabinol and its iodinated derivative in membrane bilayers Biochim. Biophys Acta 1237: 183–188
42. Mavromoustakos T, Yang DP, Makriyannis A (1995) Effects of the anesthetic steroids alphaxalone and its inactive analog Δ16-analog on the thermotropic properties of membrane bilayers. Amodel for membrane perturbation. Biochim Biophys Acta 1239:257–264
43. Mavromoustakos T, De-Ping Y, Makriyannis A (1996) Topography and thermotropic properties of cannabinoids in brainsphingomyelin bilayers. Life Sci 59:1969–1979
44. Mavromoustakos T, Theodoropoulou E, Papahatjis D, Kourouli T, De-Ping Y, Trumbore M, Makriyannis A (1996) Studies on the thermotropic effects of cannabinoids on phosphatidylcholine bilayers using differential scanning calorimetry and small angle X-ray diffraction. Biochim Biophys Acta 1281:235–244

45. Mavromoustakos T, Theodoropoulou E, Yang DP (1997) The use of high-resolution solid-state NMR spectroscopy and differential scanning calorimetry to study interactions of anaesthetic steroids with membrane. Biochim Biophys Acta 1328:65–73
46. Mavromoustakos T, Papahatjis D, Laggner P (2001) Differential membrane fluidization by active and inactive cannabinoid analogs. Biochim Biophys Acta 1512:183–190
47. Koukoulitsa C, Durdagi S, Siapi E, Villalonga-Barber C, Alexi X, Sttele BR, Screttas MM, Alexis MN, Kakoulidou AT, Mavromoustakos T (2011) Comparison of thermal effects of stilbenoid analogs in lipid bilayers using differential scanning calorimetry and molecular dynamics:correlation of thermal effects and topographical position with antioxidant activity. Eur Biophys J 40:865–875
48. Braunschweiler L, Ernst RR (1983) Coherence transfere by isotropic mixing: application to proton correlation spectroscopy. J Magn Reson 53:521–528
49. Jeener J, Meier BH, Bachmann P, Ernst RR (1979) Investigation of exchange proccesses by two-dimensional NMR spectroscopy. J Chem Phys 71:4546–4553
50. Discovery Studio v1.7, a molecular modeling system, supplied by Accelrys Inc., San Diego, CA
51. Mayo SL, Olafson BD, Goddard WA (1990) DREIDING: A Generic Force Field for Molecular Simulations. J Phys Chem 94: 8897–8909
52. van Der Spoel D, Lindahl E, Hess B, Groenhof G, Mark AE, Berendsen HJ (2005) GROMACS: fast, flexible, and free. J Comput Chem 26:1701–1717
53. van Gunsteren WF, Billeter SR, Eising AA, Hunenberger PH, Kruger P, Mark AE, Scott WRP, Tironi IG (1996) Biomolecular Simulation: the GROMOS96 Manual and User Guide; Vdf Hochschulverlag AG an der ETH Zurich
54. Essmann U, Perera L, Berkowitz ML, Darden T, Lee H, Pedersen LG (1995) A smooth particle mesh Ewald method. J Chem Phys 103:8577–8593
55. Hess B, Bekker H, Berendsen HJC, Fraaije JGEM (1997) LINCS: a linear constraint solver for molecular simulations. J Comput Chem 18:1463–1472
56. Humphrey W, Dalke A, Schulten K (1996) VMD: visual molecular dynamics. J Mol Graph 14:33–38
57. Sastry M, Lowrie JF, Dixon SL, Sherman W (2010) Large-scale systematic analysis of 2D fingerprint methods and parameters to improve virtual screening enrichments. J Chem Inf Model 50: 771–784
58. MacroModel, version 9.8; Schrödinger, LLC: New York, NY, 2010
59. LigandScout 3.0, Inte:Ligand, Software-Entwicklungs und Consulting GmbH: Vienna, Austria, 2010